Remote Sensing of Environment 190 (2017) 178–187

Contents lists available at ScienceDirect

Remote Sensing of Environment

journal homepage: www.elsevier.com/locate/rse

Application of satellite solar-induced chlorophyll fluorescence to understanding large-scale variations in vegetation phenology and function over northern high latitude forests

Su-Jong Jeong [a,*,1], David Schimel [a], Christian Frankenberg [a], Darren T. Drewry [a,e], Joshua B. Fisher [a], Manish Verma [a,2], Joseph A. Berry [b], Jung-Eun Lee [c], Joanna Joiner [d]

[a] Jet Propulsion Laboratory, California Institute of Technology, Pasadena, CA 91109, USA
[b] Department of Global Ecology, Carnegie Institution of Washington, 260 Panama Street, Stanford, CA 94305, USA
[c] Department of Geological Sciences, Brown University, Providence, RI, USA
[d] NASA Goddard Space Flight Center, Greenbelt, MD, USA
[e] Joint Institute for Regional Earth System Science and Engineering, University of California, Los Angeles, California, USA

ARTICLE INFO

Article history:
Received 30 October 2015
Received in revised form 29 October 2016
Accepted 27 November 2016
Available online xxxx

Keywords:
Solar-induced chlorophyll fluorescence
SIF
NDVI
GPP
Phenology
Large-scale

ABSTRACT

This study evaluates the large-scale seasonal phenology and physiology of vegetation over northern high latitude forests (40°–55°N) during spring and fall by using remote sensing of solar-induced chlorophyll fluorescence (SIF), normalized difference vegetation index (NDVI) and observation-based estimate of gross primary productivity (GPP) from 2009 to 2011. Based on GPP phenology estimation in GPP, the growing season determined by SIF time-series is shorter in length than the growing season length determined solely using NDVI. This is mainly due to the extended period of high NDVI values, as compared to SIF, by about 46 days (±11 days), indicating a large-scale seasonal decoupling of physiological activity and changes in greenness in the fall. In addition to phenological timing, mean seasonal NDVI and SIF have different responses to temperature changes throughout the growing season. We observed that both NDVI and SIF linearly increased with temperature increases throughout the spring. However, in the fall, although NDVI linearly responded to temperature increases, SIF and GPP did not linearly increase with temperature increases, implying a seasonal hysteresis of SIF and GPP in response to temperature changes across boreal ecosystems throughout their growing season. Seasonal hysteresis of vegetation at large-scales is consistent with the known phenomena that light limits boreal forest ecosystem productivity in the fall. Our results suggest that continuing measurements from satellite remote sensing of both SIF and NDVI can help to understand the differences between, and information carried by, seasonal variations vegetation structure and greenness and physiology at large-scales across the critical boreal regions.

1. Introduction

Over northern temperate and boreal forests, vegetation has a clear seasonal cycle in its annual growth (Myneni et al., 1997). Seasonal processes, including spring green-up and fall senescence, control growing season length and therefore have a significant influence on photosynthetic CO_2 uptake from the atmosphere. In the Northern Hemisphere, seasonal activity of vegetation controls the observed seasonal cycle of atmospheric CO_2 (Keeling et al., 1996). Increases in temperature over cold temperate and boreal forests have the potential to influence atmospheric CO_2 seasonality globally (Denning et al., 1995; Graven et al., 2013). Therefore, understanding the seasonal dynamics of boreal zone vegetation is a key step in comprehending the seasonal response of atmospheric CO_2 to global and/or regional warming.

In characterizing the seasonal dynamics of vegetation, many researchers have focused on the timing of specific events (phenology) such as spring flowering, budburst, fall leaf coloring, and leaf drop (see review by Richardson et al., 2013). Many studies from various ground measurements with different species found dominant changes in spring phenology in response to temperature and/or precipitation variability over mid- to high-latitude forests (Ho et al., 2006; Menzel et al., 2006; Schwartz et al., 2006; Wolkovich et al., 2012; Fu et al., 2015; Piao et al., 2015). Although limited studies have focused on fall phenology, apparent variations in the timing of leaf coloring and drop in relation to temperature variations have been reported (Lee et al., 2003; Delpierre et al., 2009; Archetti et al., 2013; Jeong & Medvigy, 2014). It is expected that global and/or regional climate change will

* Corresponding author.
E-mail address: waterbell77@gmail.com (S.-J. Jeong).
[1] School of Environmental Science and Engineering, South University of Science and Technology, Shenzhen, China.
[2] Consulting for Statistics, Computing, and Analytics Research University of Michigan Ann Arbor, MI, USA.

http://dx.doi.org/10.1016/j.rse.2016.11.021
0034-4257/

lead to an increase in growing season length through earlier spring onset or delayed fall senescence (e.g., Morin et al., 2009; Jeong et al., 2013).

Satellite remote sensing of vegetation has the potential to greatly improve our understanding of northern latitude forests, particularly their seasonal productivity, reflectance-based indices such as the normalized difference vegetation index (NDVI) has been widely used to understand the phenology and vegetation growing season from regional to the global scales (de Beurs & Henebry, 2005; Piao et al., 2006; White et al., 2009; Jeong et al., 2011; Barichivich et al., 2013; De Jong et al., 2013; Melaas, Friedl, & Zhu, 2013). NDVI-based studies also showed clear changes in spring and fall phenology related to temperature or precipitation changes (Fu et al., 2014; Shen et al., 2015). For example, increasing winter and spring temperatures can lead to earlier green-onset or increase in summer, and fall temperature delays the timing of leaf drop and reductions in greenness over the Northern Hemisphere (Jeong et al., 2011). Satellite remote sensing of NDVI is a widely used tool to understand the continuous temporal trajectory of vegetation growth and decay over the entire globe (Tucker et al., 1986; Xu et al., 2013; Buitenwerf et al., 2015; Park et al., 2015).

As a benefit of temporal and spatial coverage, satellite NDVI-based phenology is used to understand the relationships between vegetation growing season and vegetation carbon assimilation, or gross primary productivity (GPP) (e.g., Jeong et al., 2013; Keenan et al., 2014). Particularly in regions with minimal ground measurements, satellite-based phenology has tremendous potential to provide insights and monitoring capabilities for vegetation seasonal growth and productivity. However, previous studies which compare satellite NDVI data with tower-measured CO_2 flux data from FLUXNET (GPP and net ecosystem exchange (NEE)) (Churkina et al., 2005; Gonsamo et al., 2012) have found that the NDVI-based growing season is longer than the duration of flux measurements, suggesting a discrepancy in seasonality between vegetation greenness and function (Churkina et al., 2005). These discrepancies could be due to the differences in the scales between satellite and tower measurements, rather than actual offsets in time between greenness (or structure) and function (Cescatti et al., 2012), and so additional observations are required to help resolve these issues.

Recently, large-scale satellite remote sensing of solar-induced chlorophyll fluorescence (SIF) has become available (Meroni et al., 2009; Frankenberg et al., 2011; Joiner et al., 2011). SIF is the re-emission of a small fraction of absorbed radiation, at longer wavelengths that extend into the near infrared. SIF has been theoretically related to photosynthetic activity by way of complex mechanisms of energy dissipation (Krause and Weis, 1991; Zhang et al., 2014). Several studies have shown an almost linear relationship between SIF and GPP (Van der Tol et al., 2009, Zarco-Tejada et al., 2013) In general, about 1% of the solar energy captured by plants is reemitted by chlorophyll as fluorescence. This relatively small amount of radiation is detectable from space with current high spectral resolution sensors, essentially providing a distinctive "glow" of photosynthetically active vegetation at wavelengths between approximately 640 nm and 820 nm. New spectrometers with high spectral resolution, in combination with advances in retrieval methodology based on the exploitation of Fraunhofer lines, now enable global SIF retrievals from platforms such as the Global Ozone Monitoring Instrument-2 (GOME-2) (Joiner et al., 2011), Greenhouse gases Observing SATellite (GOSAT) (Frankenberg et al., 2011), and Orbiting Carbon Observatory (OCO2) (Frankenberg et al., 2014). At canopy- and ecosystem-scale, compared to reflectance-based vegetation indices, changes in SIF provide insight into plant physiological functioning. Thus, satellite-based SIF observations offer an alternative view of vegetation function based on physiology, as opposed to the information on structure and greenness offered by traditional reflectance indices.

Studies on SIF from leaf to canopy-scale show a positive relationship between SIF and photosynthesis (Van der Tol et al., 2009, Zarco-Tejada et al., 2013; Guanter et al., 2014; Damm et al., 2015). Remote sensing of SIF also correlated well with ground-based SIF measurements and GPP from flux-towers over temperate and boreal forests (Joiner et al., 2014; Yang et al., 2015). In addition, Lee et al. (2013) show that SIF can capture a decline in photosynthesis in a drought-stressed forest even as leaf area remained constant, confirming that the passive measurements of SIF can be used to track changes in physiological activity at large scales in the absence of changes in greenness or structure. Several ground-based studies of SIF have also shown a positive correlation between SIF and water stress (Flexas et al., 2002; Daumard et al., 2010).

The applicability of satellite SIF to provide insights or a monitoring capability for seasonal changes in vegetation function is not yet well developed, particularly at large scales from region to the globe. Because of the highly non-linear characteristics of terrestrial ecosystem dynamics across scale (Heffernan et al., 2014), it has the potential to modify local-scale observations of positive relationships between SIF and GPP seasonality. In this study we examine the potential of SIF to provide unique information on the seasonal dynamics of northern latitude forests, by comparing satellite remote sensing of SIF, NDVI, and a validated data-driven model of GPP. We focus on two different characteristics of the seasonal dynamics of vegetation: structural phenology and physiology. A recent study comparing the temperature responses of NEE and GPP to across the growing season revealed a hysteresis in NEE response to temperature between spring and fall in northern latitude forests (Niu et al., 2013). This difference was primarily attributed to the different responses of GPP to temperature changes rather than those of ecosystem respiration. Here, we build on this result to examine the value of satellite-based SIF observations to characterize boreal forest physiological activity over the northern latitude growing season, with a particular focus on responses to seasonal temperature variations.

2. Data and methods

In this study, we used satellite remote sensing of NDVI and SIF from two different sources. For NDVI, we used the new Global Inventory Modeling and Mapping Studies (GIMMS) NDVI3g data from the Advanced Very High Resolution Radiometer (AVHRR) sensor (Pinzon and Tucker, 2014) that has been widely used for evaluating ecosystem changes (e.g., Bhatt et al., 2013; De Jong et al., 2013; Zhu et al., 2013; Dardel et al., 2014). In addition, we used Moderate Resolution Imaging Spectroradiometer (MODIS) NDVI data (MOD13C2), which samples with narrower spectral bands. Compared to the AVHRR, the MODIS NDVI is based on spectral bands specifically designed for vegetation monitoring and includes improved radiometric sensitivity, atmospheric corrections, and reduced geometric distortions (Huete et al., 2002).

We used two different SIF datasets from the Global Ozone Monitoring Instrument - 2 (GOME-2) (Joiner et al., 2011) and the Greenhouse gases Observing SATellite (GOSAT) (Frankenberg et al., 2011). GOME-2 is a nadir-viewing grating spectrometer that measures backscattered sunlight at wavelengths between 270 and 800 nm on board the MetOp-A platform, which was launched in October 2006 in a sun-synchronous orbit with an equator crossing time of 09:30 AM. The nadir Earth footprint size is 40 × 80 km, and the normal swath is 1920 km. GOME-2 SIF primarily comes from the filling-in of solar Fraunhofer lines near the 740 nm far-red fluorescence emission peak as shown in Joiner et al. (2013). The GOME-2 SIF retrieval method uses principal component analysis with a simplified radiative transfer model to disentangle the spectral signatures of atmospheric absorption, surface reflectance, and fluorescence emission. All data has been cloud filtered and eliminated with solar zenith angle >70. In this study, we used Level 3 global-scale grid averaged (0.5° × 0.5°) data (Joiner et al., 2013).

In case of GOSAT SIF, high-resolution spectra are recorded by the thermal and near infrared sensor for carbon observation (TANSO) Fourier transform spectrometer (FTS) on board the Japanese GOSAT satellite, which was launched in January 2009 into a sun-synchronous orbit with a local overpass time of 13:00 PM. Approximately 10,000 soundings with circular spatial footprint (10 km diameter) are recorded

daily, repeating a regularly spaced global grid every 3 days. GOSAT retrieved steady-state solar induced chlorophyll fluorescence based on in-filling of Fraunhofer lines at 757 and 771 nm, as described in Frankenberg et al. (2011). The GOSAT SIF data was also cloud filtered prior to application here. In this study, we used the global-scale grid averaged (1° × 1°) SIF data from Frankenberg et al. (2011) to reduce the noise in original pixel data.

For this analysis we used two different GPP data sets. The "data-driven" GPP product is a statistical model result produced at the Max Planck Institute (MPI) for Biogeochemistry (Jung et al., 2011). We also use a "semi-empirical" GPP product obtained from the Moderate Resolution Imaging Spectroradiometer (MODIS) MOD17 GPP model (Running et al., 2004). Both MPI- and MODIS-GPP represent ecosystem-level GPP relatively well (Running et al., 2004, Jung et al., 2011).

We used incoming shortwave radiation (SWR) and temperature to provide information on the environmental conditions responsible for seasonal variations in vegetation. SWR data was obtained from the National Aeronautics and Space Administration's (NASA) Clouds and the Earth's Radiant Energy System (CERES) down-welling all-sky SWR at the surface (EBAF-Surface) (Caldwell et al., 2008). The temperature data used in this study is the Climate Research Unit time-series 3.21 climate data from the University of East Anglia (Harris et al., 2013).

We focused on the northern temperate and boreal forests from 40° to 55°N in Eurasia and North America to match with the limitations in the GOSAT winter data (available up to 55°N). The area includes evergreen needleleaf, evergreen broadleaf, deciduous needleleaf, deciduous broadleaf, and mixed forests according to the land cover classification of the International Geosphere Biosphere Program (IGBP). We used monthly data for a 3-year period (2010 − 2012). This time period was chosen due to the availability of all of the datasets used in this study. More details about the data used in this study are presented in Table 1.

To compare the phase of seasonal cycle among data sets, we first aggregated all data to a 1° × 1° grid to match the coarsest resolution among all data sets (e.g., CERES). Next, we used the normalized year-round monthly values by using the annual maximum and minimum over the entire area between 40 and 55°N across both North America and Eurasia (Figs. 1–4). To evaluate the differences in spring and fall events between NDVI-, SIF-, and GPP-based seasonal cycle (Figs. 4–5), we first calculated the start and end of a growing season (e.g., spring onset and fall offset) using three different thresholds (20%, 50%, and 80% of annual maximum) to correspond to a range of developmental stages (Richardson et al., 2012). For example, the first spring day is defined as the date when the seasonal NDVI (SIF and GPP) reaches 20% of the annual maximum, whereas the last fall day is defined as the date when the seasonal NDVI (SIF and GPP) drops to 20% of the annual maximum. These threshold dates for spring and fall were estimated by fitting a 6-degree polynomial to the monthly data. This method has been widely used in NDVI-based phenology studies (e.g., Yongshuo et al., 2014). More details on these phenology methods are described in Jeong et al. (2011). After estimating spring and fall dates in each data, we made a representative spring and fall dates by averaging two different spring (fall) dates from two remote sensing data in each variable (i.e., SIF spring dates is estimated by averaging over two different spring dates from GOME-SIF and GOSAT-SIF).

3. Results

We first compared the normalized seasonal cycles of NDVI with SIF and GPP over Eurasia and North America for the period 2010–2012 (Fig. 1a and b, respectively). Over the two continents, the seasonal cycles of NDVI for both MODIS and GIMMS show a longer season than that of SIF for both GOSAT and GOME (Fig. 1a). In the spring NDVI can be seen to rise earlier than SIF, and in the fall NDVI reduces later in the year relative to SIF. Between seasons, differences between normalized NDVI and SIF are much larger in fall than in spring. For example, in Eurasia, differences in the normalized monthly values between NDVI and SIF in October (−0.51 for GOSAT SIF minus MODIS NDVI and −0.49 for GOSAT SIF minus GIMMS NDVI) are more than twice those in April (−0.21 for GOSAT SIF minus MODIS NDVI and −0.17 for GOSAT SIF minus GIMMS NDVI). These comparisons are averaged over the entire area between 40 and 55°N across both North America and Eurasia (Fig. 1). But, even when we divided this area by 5-degree latitude intervals, the overall patterns of difference between SIF and NDVI remain similar, though with difference in magnitudes. SIF captures the seasonal cycle of both MPI and MODIS GPP. This similarity in the seasonal cycle between SIF and GPP is observed over both Eurasia and North America (Fig. 1a and b). In contrast to SIF, the seasonal cycle of NDVI is somewhat different from the seasonal cycle of GPP for both continents using either MODIS or GIMMS. In addition, when we divided the entire domain by two dominant plant functional types in this region (e.g., deciduous and evergreen forests, respectively), the differences between SIF, NDVI and GPP are still observed in both deciduous and evergreen forests (Fig. 2).

Here, it should be noted that dominant differences in monthly values between SIF and NDVI are still observed after normalizing each month by the respective monthly standard deviation (SD) for 3-yr period. For example, in the spring phase, monthly SDs for normalized SIF are 0.04, 0.03, 0.04, from April to June for normalized GOME SIF, and are 0.05, 0.02, 0.03 from April to June for SIF GOSAT. On the other hand, monthly SDs for normalized NDVI are 0.01, 0.03, 0.01, from April to June for normalized MODIS NDVI, and are 0.03, 0.01, 0.02 from April to June for SIF GOSAT. Estimated SDs from NDVI and SIF are less than the range of difference of normalized NDVI and SIF. Thus, it is not likely that the monthly differences are due to inter-annual variability, although it cannot be confirmed from a short record used in the present study. On the other hand, differences of monthly values between GOME and GOSAT SIF or between MODIS and GIMMS NDVI are less than the magnitude of variability of each data. Then, differences of seasonality between SIFs (or NDVIs) are not statistically significant.

Next, we examined seasonal variations in incoming SWR and temperature versus SIF and NDVI to see the relationship between the seasonality of the environment across these regions and the remotely

Table 1
Description of NDVI, SIF, GPP, radiation, and temperature data in this study.

Variable	Origin	Temporal resolution	Spatial resolution	Reference
NDVI (normalized difference vegetation index)	GIMMS (Global Inventory Modeling and Mapping Studies)	15-day	8 km × 8 km	Pinzon and Tucker (2014)
	MODIS (Moderate Resolution Imaging Spectroradiometer)	Monthly	0.05° × 0.05°	Huete et al. (2002)
SIF (solar-induced chlorophyll fluorescence)	GOSAT (Greenhouse gases Observing SATellite)	Monthly	1.0° × 1.0°	Frankenberg et al. (2011)
	GOME (Global Ozone Monitoring Instrument-2)	Monthly	0.5° × 0.5°	Joiner et al. (2011)
GPP (gross primary productivity)	MPI-BGC (Max Planck Institute for Biogeochemistry)	Monthly	0.5° × 0.5°	Jung et al. (2011)
	MODIS (Moderate Resolution Imaging Spectroradiometer)	Monthly	0.5° × 0.5°	Running et al. (2004)
Incoming shortwave radiation	CERES (Clouds and the Earth's Radiant Energy System)	Monthly	1.0° × 1.0°	Caldwell et al. (2008)
Temperature	CRU (Climate Research Unit time-series 3.21)	Monthly	0.5° × 0.5°	Harris et al. (2013)

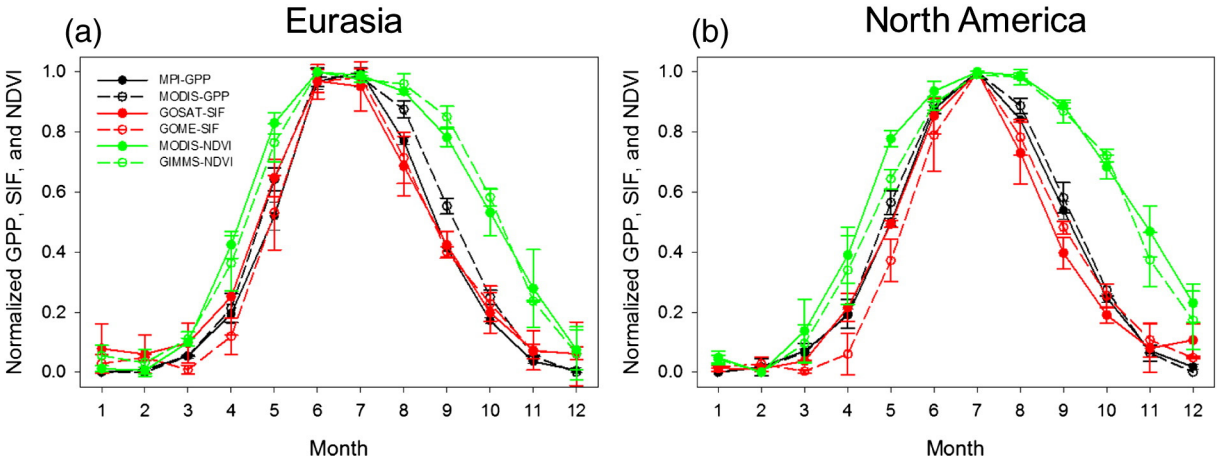

Fig. 1. Normalized mean seasonal cycle of area averaged GOSAT SIF, GOME SIF, MODIS NDVI, GIMMS NDVI, MPI GPP, and MODIS GPP over northern temperate and boreal forests (40–55°N) for the period 2010–2012 in Eurasia (a) and in North America (b). Error bars in all figures indicate monthly standard deviations for the period 2010–2012.

sensed variables (Fig. 3). At both of two continents, in spring, seasonal evolution of NDVI and SIF lagged behind that of temperature and SWR. On the contrary, in fall, after reaching the annual maximum, SIF falls as the radiation forcing decreases, whereas NDVI and temperature see higher values that extend further into the fall season. Overall, in contrast to NDVI, as a physiological response variable, SIF implicitly includes the impacts of temperature as well as aspects of radiation availability at large-scale.

We further quantified differences in the timing of phenology events in the spring and fall (i.e., spring/fall onset/offset or start/end of growing season) between NDVI, SIF, and GPP (Fig. 4). Here, we also estimated spring and fall dates by calculating NDVI × SWR to understand the impact of radiation availability. In spring, over Eurasia, regardless of the selected threshold values (e.g., 20, 50, and 80%, respectively), NDVI-based onset dates increase in spring before SIF- and GPP-based onset dates for all latitude bands (upper panel in Fig. 4). Averaged over the latitude bands, the spring onset date of NDVI for the 20% threshold (day of year: DOY 76 (±17 days)) precedes SIF and GPP by 24 (±6) days and 23 (±9) days, respectively. However, the spring initiation of SIF (DOY 100 (±8 days) for 20% threshold, DOY 126 (±7 days) for 50% threshold, and DOY 154 (±9 days) for 80% threshold corresponds to spring initiation of GPP DOY 99 (±11 days) for 20% threshold, DOY 125 (±7 days) for 50% threshold, and DOY 153 (±9 days) for 80% threshold. In contrast to spring days, the fall days for NDVI lag the days from SIF and GPP by 46 (±11 days) and 43 (±8 days) days, respectively. These general differences between SIF and NDVI onset and offset days are observed in North America as well, indicating that the two types of measurements observe fundamentally different phenomena with information on contrasting aspects of system function.

Consequently, NDVI-based phenology shows longer growing seasons than those derived from SIF- or GPP-based phenology. In particular, the differences in fall offset dates between NDVI and SIF (or GPP)

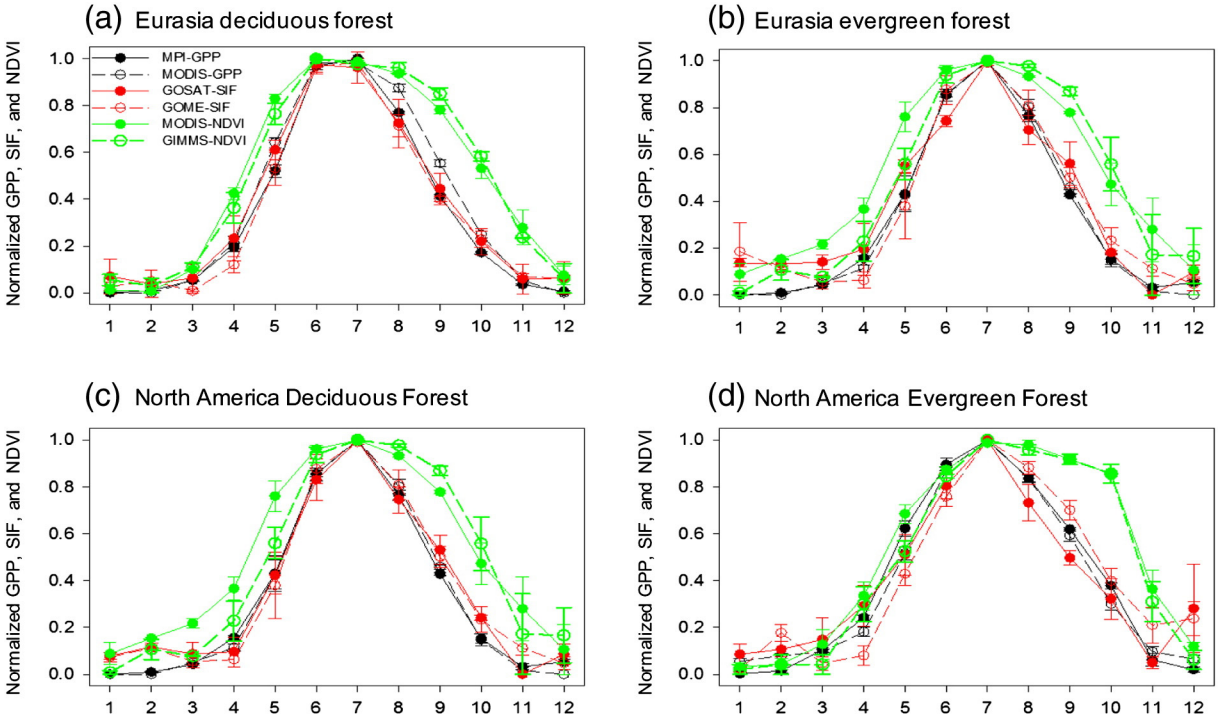

Fig. 2. Normalized mean seasonal cycle of area averaged GOSAT SIF, GOME SIF, MODIS NDVI, GIMMS NDVI, MPI GPP, and MODIS GPP over northern temperate and boreal forests (40–55°N) for the period 2010–2012 in deciduous and evergreen forests over Eurasia (a, b) and over North America (c, d). Error bars in all figures indicate monthly standard deviations for the period 2010–2012.

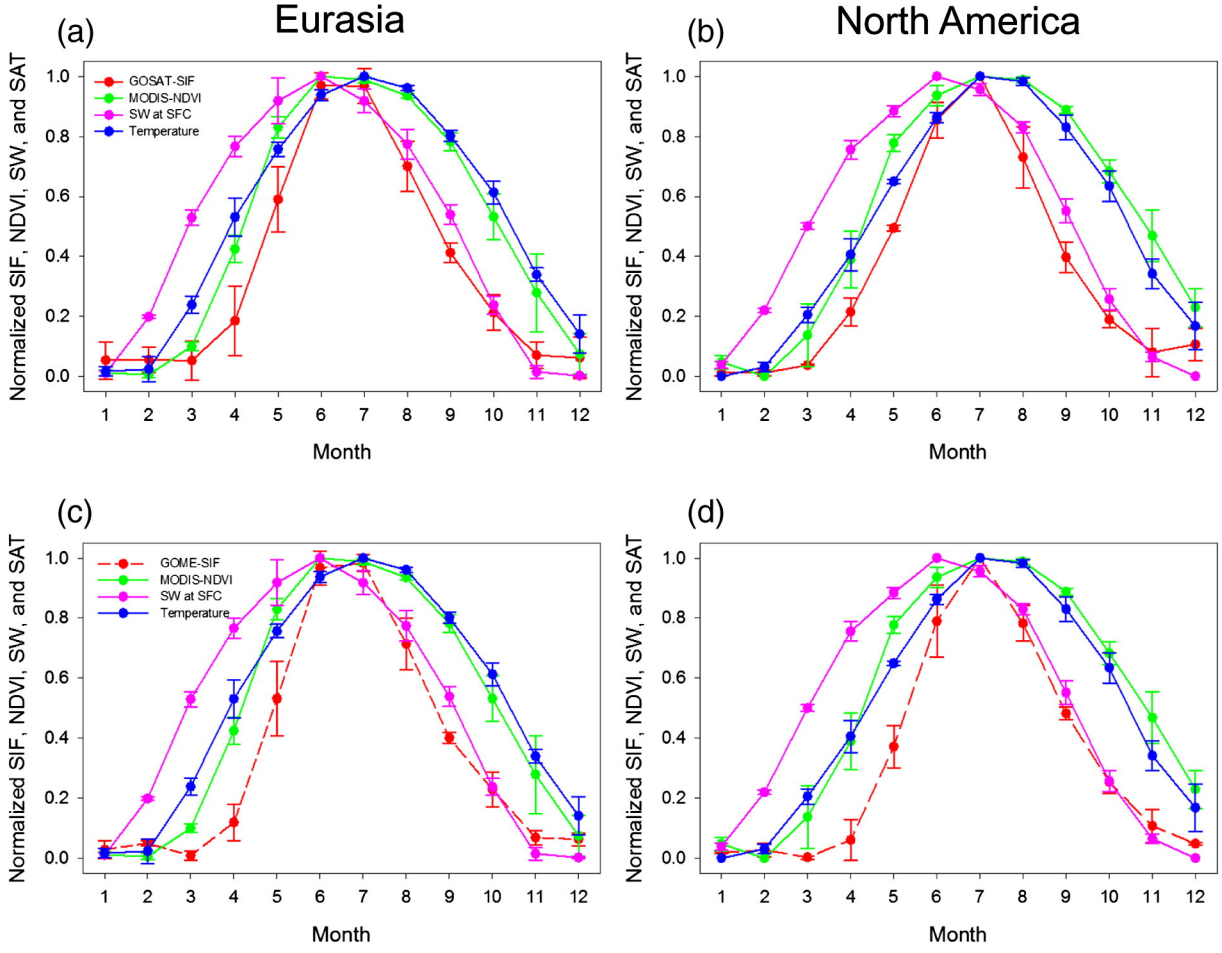

Fig. 3. Normalized mean seasonal cycle of area-averaged SIF, NDVI, incoming shortwave radiation at surface, and surface air temperature (SAT) over northern temperate and boreal forests (40–55°N) for the period 2010–2012 in Eurasia (a, c) and in North America (b, d). Error bars in all figures indicate monthly standard deviations for the period 2010–2012.

are apparent. Here, one interesting point to note is that latitudinal distributions of phenology dates of NDVI × SWR are much closer to those of SIF (or simulated GPP) in fall, suggesting fall phenology from NDVI improved when constrained by reduced radiation availability.

Difference of spring onset and fall offset dates between NDVI- and SIF-based estimations is evenly distributed over the Northern Hemisphere (Fig. 5). For example, as seen in the spatial distributions of 50% thresholds in NDVI- and SIF-based spring (Fig. 5a and b, respectively) and 50% thresholds in fall dates (Fig. 5d and e, respectively), the differences between NDVI- and SIF-based phenology dates are evenly distributed for both spring (Fig. 5c) and fall (Fig. 5d) over most parts of the analysis domains including the 5 different vegetation types in this study (Fig. 5c and f). These results indicate general differences between NDVI- and SIF-based phenology regardless of vegetation types and phenological stage. This is consistent with a recent study on the comparison between FLUXNET-GPP and remote sensing SIF among vegetation types (Joiner et al., 2014).

We evaluated the differences in the relationships between NDVI, SIF, and GPP and temperature between spring and fall (Fig. 6). In general, vegetation function and structure (including greenness and biomass) seasonality in cold temperate and boreal regions primarily vary with temperature (Piao et al., 2007). Temperature drives the majority of the seasonality seen in NDVI, SIF, and GPP. In the case of GPP, regardless of region, there is a clear difference in the spring and fall temperature response in both the MPI and MODIS GPP estimates. However, the sensitivity of GPP to temperature in spring is much larger than that in fall. In MPI-GPP, spring sensitivity is higher than in the fall by 35% in Eurasia and by 37% in North America. These seasonal differences in temperature correlations are also observed in MODIS GPP. Additionally, although we used a linear relation between GPP and temperature, GPP steeply increases when temperature reaches 9–10 °C in spring in both MPI and MODIS data, suggesting the presence of significant nonlinearity.

Both GOSAT and GOME SIF indicate that temperature sensitivity in spring is larger than in fall, likely due to the radiation constraint mentioned above. In Eurasia, the spring GOSAT-SIF (0.03 $Wm^{-2}\mu m^{-1} sr^{-1}$/°C) is three times larger than that in fall (0.01 $Wm^{-2}\ \mu m^{-1}\ sr^{-1}$/°C). Although SIF sensitivities are different between GOSAT and GOME, both datasets show consistent trends. In contrast to the modeled GPP and SIF, the NDVI responses to temperature changes in spring (0.02/°C) are the same as those in fall (0.02/°C), regardless of satellite differences. The NDVI data (GIMMS and MODIS) shows increases with temperature increases for both seasons. In spring, with available incoming solar radiation, both NDVI and SIF increased with temperature. However, in fall, the increase in temperature led to NDVI increases even in the absence of available incoming solar radiation. Overall, our results on the GPP/SIF response to temperature are consistent with previous site-level studies on temperate and boreal forests from 40 to 61°N (Niu et al., 2013).

4. Discussion and conclusions

There are systematic differences in the seasonal cycle of NDVI and SIF (or GPP) over the northern high latitude forests (Figs. 1–3). We showed that NDVI shows spring increases by about 2 weeks earlier start than that does SIF (or GPP). NDVI also has an extended period of high values, with values falling approximately 5 weeks after SIF and simulated GPP start to decline in the fall (Figs. 4–5), in both continents.

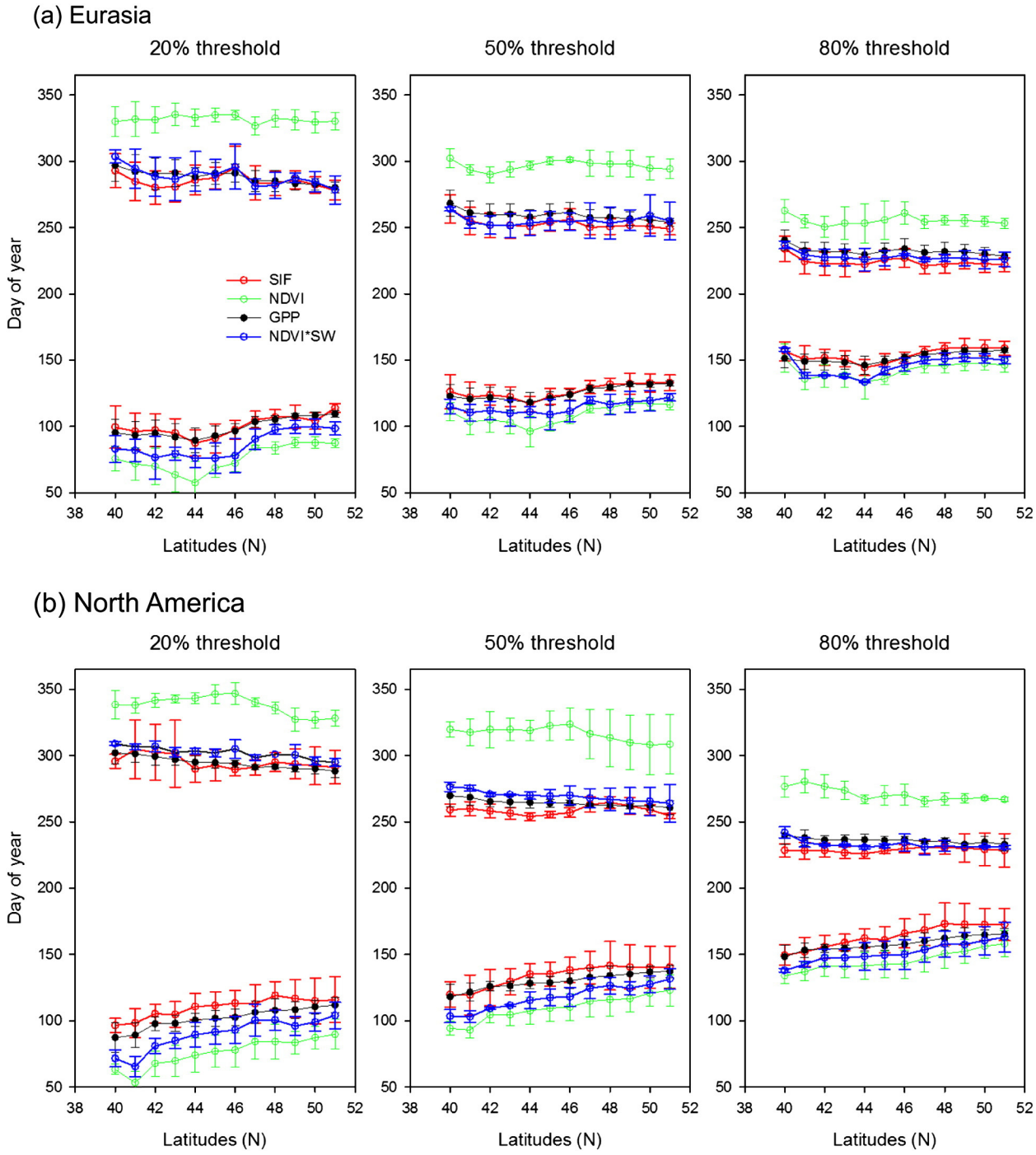

Fig. 4. The area-averaged spring and fall dates (20%, 50%, and 80% of annual maximum) of NDVI, SIF, and GPP over northern temperate and boreal forests for the period 2010–2012 in Eurasia (a) and in North America (b). The solid line (error bars) in all figures indicates mean (standard deviations) for the period 2010–2012.

Differences in the seasonal cycle of NDVI and SIF could be explained by the differences in the timing between leaf growth/decay, availability of sunlight and temperature, and the likely start of physiological activity (photosynthesis) which trails spring leaf development. Vegetation requires time to increase primary productivity by assimilating carbon after leaf emergence in spring. Thus, the timing of carbon assimilation lags behind leaf emergence and varies with leaf structure, habit, and longevity (Kikuzawa, 2003). This is consistent with our observations that spring SIF trends lag behind NDVI-based spring phenology. However, in fall, photosynthesis shuts down before leaf coloration (Daumard et al., 2010). This is because fall carbon assimilation of boreal coniferous (Suni et al., 2003) and temperate forests (Medvigy et al., 2013) are limited by light availability. But, autumn leaf chlorophyll reduction and leaf drop is affected by temperature variability, after photosynthesis has begun to diminish (Jeong and Medvigy, 2014). This is consistent with NDVI-based fall phenology lagging behind SIF-based fall phenology in the present study.

Results on the phenological differences between NDVI and SIF are consistent with flux measurements showing that the satellite NDVI-based growing season is longer than the duration of carbon uptake (Churkina et al., 2005). In contrast, the SIF-based growing season shows almost the same phenological pattern as GPP across latitudes and continents (Figs. 4 and 5). The seasonal cycle of SIF is well correlated with that of GPP, confirming previous leaf-level and site-level positive

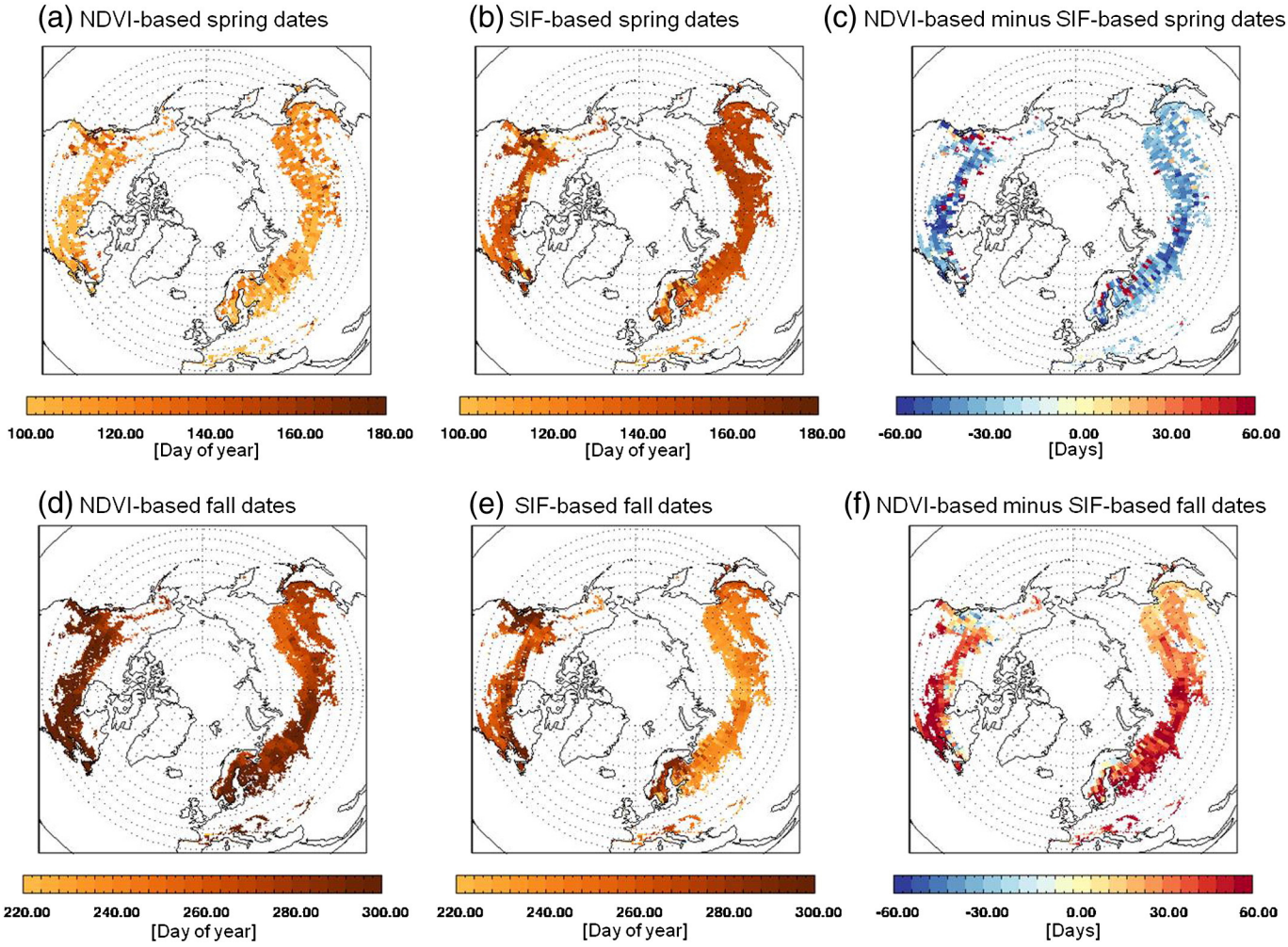

Fig. 5. Spatial distributions of 3-year mean (2010–2012) NDVI- and SIF-based phenology dates (50% threshold) for spring (a, b) and fall (d, e), difference between NDVI- and SIF-based phenology dates for spring (c) and fall over Northern Hemisphere.

relationships between SIF and GPP (Van der Tol et al., 2009; Zarco-Tejada et al., 2013; Guanter et al., 2014, Joiner et al., 2014). For example, in an agricultural system, Zarco-Tejada et al. (2013) showed close relationships across the seasonal cycle between GPP and physiological variables such as chlorophyll fluorescence and chlorophyll content, whereas vegetation indices such as NDVI are related to the canopy structure which can show lags in correlation with physiological variables. Two recent studies, which used the same SIF products as were used in this study, showed clear correlations in the seasonality of satellite-based SIF, ground-based SIF (e.g., Yang et al., 2015) and tower-measured GPP (e.g., Joiner et al., 2014) over temperate and Boreal forests in our analysis domain. These results suggest that SIF can be used as a direct observation of the large-scale "phenology of physiology" from leaf- to global-scale. This is very important for understanding the global carbon cycle, because our understanding of the functional growing season is limited to biomes and latitudes sampled by FLUXNET sites (Schimel et al., 2015), and the boreal regions are dramatically undersampled by in-situ systems relative to their tremendous importance in the global carbon cycle.

Differences or similarities of the seasonal cycle between NDVI and SIF have strong implications for uncertainties in simulated terrestrial carbon budget in process-based terrestrial ecosystem models. Recently, the North American Carbon Program synthesis studies showed significant biases in NEE (Schwalm et al., 2010), GPP (Schaefer et al., 2012), and phenology (Richardson et al., 2012) in the spring and fall. Process-based models (e.g., terrestrial ecosystem models; Fisher et al., 2014) often use remote sensing of NDVI for representing plant seasonal cycle and overestimate GPP compared to observations, especially in spring and fall (Schaefer et al., 2012). This is consistent with a model bias for a longer growing season compared to observations (Richardson et al., 2012). Our results indicate that terrestrial ecosystem models overestimate of GPP are likely traceable to the use of LAI (from NDVI) or NDVI-based phenology schemes. This study suggests that the SIF-based "phenology of physiology" may help to reduce biases in the simulated GPP by separating the phenology of vegetation function (by SIF) from that of vegetation structure (by NDVI or LAI) for biogeophysical process.

We also found that the sensitivity of SIF and GPP to temperature shows clear differences between the spring growth and fall senescence depicted in NDVI time series (Fig. 6). In contrast to SIF and GPP, NDVI responses to temperature do not show seasonal hysteresis. Similarly, the close relationships between GPP and SIF indicate that SIF captures the seasonal plant photosynthetic responses to temperature change. Our results suggest satellite-based SIF could be used as a more direct measurement of the seasonality of photosynthesis, with the SIF observing capability of the Orbiting Carbon Observatory (OCO2) (Frankenberg et al., 2014) offering tremendous potential to help by providing much denser SIF observations than have been previously available. Eventually, the combination of structural and physiological information from NDVI (from MODIS and GIMMS) and SIF measurements will help to improve our understanding of terrestrial ecosystems and the global carbon cycle.

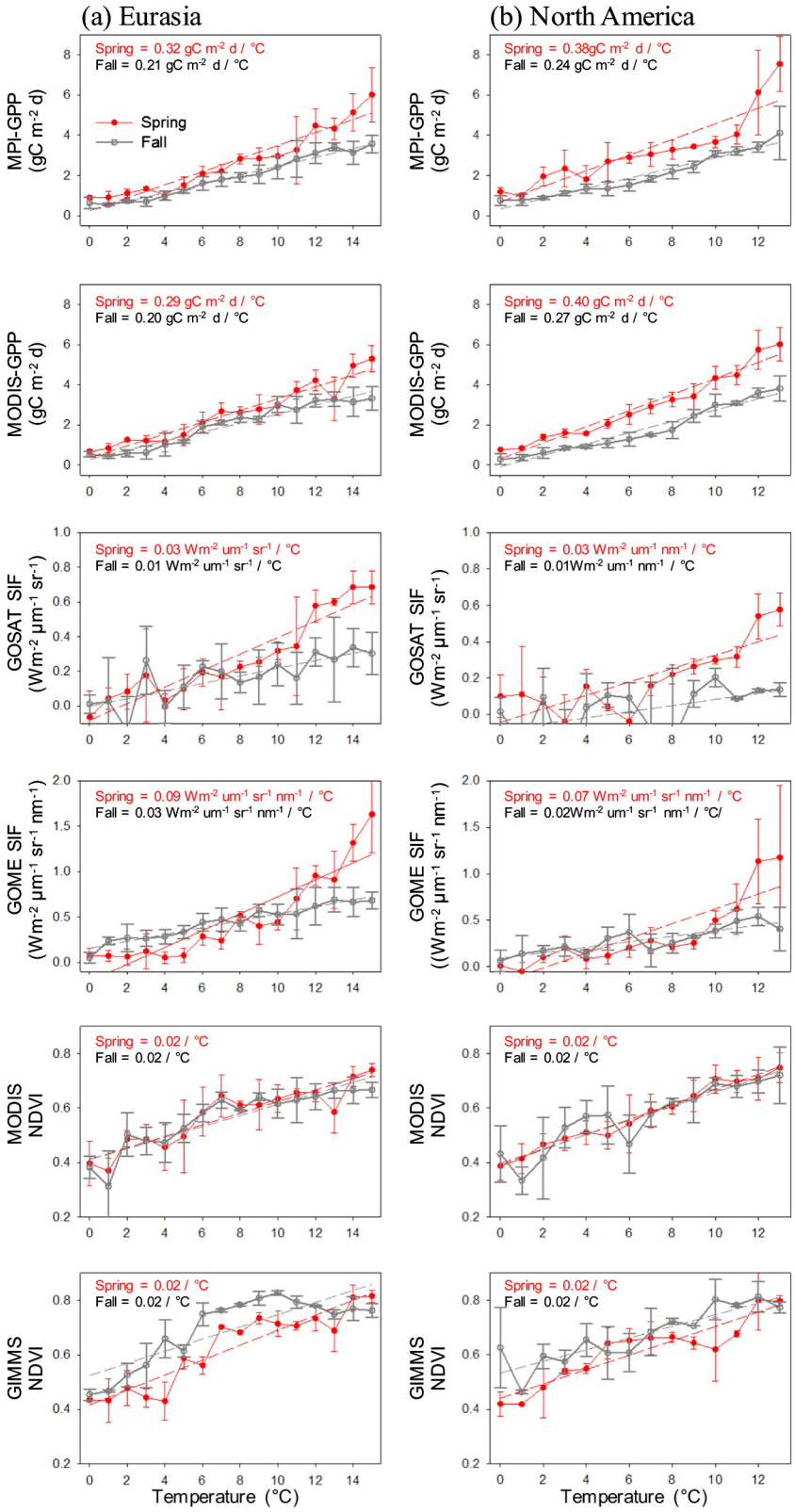

Fig. 6. A comparison of the sensitivity of GPP, NDVI, and SIF to temperature changes between spring (March–May) and fall (September–November). Each bin shows the average value of GPP and vegetation indices for 1 °C temperature interval over temperate and boreal forests (40–55°N) for the period 2010–2012 in Eurasia (a) and in North America (b). The slope is the linear regression between GPP (SIF and NDVI) and temperature. The solid line (error bars) in all figures indicates mean (standard deviations) for the period 2010–2012.

Acknowledgements

This research was carried out at the Jet Propulsion Laboratory, California Institute of Technology, under a contract with the National Aeronautics and Space Administration.

References

Archetti, M., Richardson, A.D., O'Keefe, J., Delpierre, N., 2013. Predicting climate change impacts on the amount and duration of autumn colors in a New England forest. PLoS ONE 8 (3):e57373. http://dx.doi.org/10.1371/journal.pone.0057373.

Barichivich, J., Briffa, K.R., Myneni, R.B., Osborn, T.J., Melvin, T.M., Ciais, P., et al., 2013. Large-scale variations in the vegetation growing season and annual cycle of atmospheric CO_2 at high northern latitudes from 1950 to 2011. Glob. Chang. Biol. 19, 3167–3183.

Bhatt, U.S., Walker, D.A., Raynolds, M.K., Bieniek, P.A., Epstein, H.E., Comiso, J.C., Pinzon, J.E., Tucker, C.J., Polyakov, I.V., 2013. Recent declines in warming and vegetation greening trends over Pan-Arctic tundra. Remote Sens. 5, 4229–4254.

Buitenwerf, R., Rose, L., Higgins, S.I., 2015. Three decades of multi-dimensional change in global leaf phenology. Nat. Clim. Chang. 5, 364–368.

Caldwell, T.E., Coleman, L.H., Cooper, D.L., Escuadra, J., Fan, A., Franklin, C.B., et al., 2008. Clouds and the Earth's Radiant Energy System (CERES) Data Management System Data Products Catalog. Release 4 Version 16. 240 pp., February. Available at:. http://eosweb.larc.nasa.gov/PRODOCS/ceres/DPC/.

Cescatti, A., Marcolla, B., Santhana Vannan, S.K., Pan, J.Y., Román, M.O., Yang, X., et al., 2012. Intercomparison of MODIS albedo retrievals and in situ measurements across the global FLUXNET network. Remote Sens. Environ. 121, 323–334.

Churkina, G., Schimel, D., Braswell, B.H., Xiao, X., 2005. Spatial analysis of growing season length control over net ecosystem exchange. Glob. Chang. Biol. 11, 1777–1787.

Damm, A., Guanter, L., Verhoef, W., Schläpfer, D., Garbari, S., Schaepman, M.E., 2015. Impact of varying irradiance on vegetation indices and chlorophyll fluorescence derived from spectroscopy data. Remote Sens. Environ. 156:202–215. http://dx.doi.org/10.1016/j.rse.2014.09.031.

Dardel, C., Kergoat, L., Hiernaux, P., Mougin, E., Grippa, M., Tucker, C., 2014. Re-greening Sahel: 30 years of remote sensing data and field observations (Mali, Niger). Remote Sens. Environ. 140, 350–364.

Daumard, F., Champagne, S., Fourier, A., Goulas, Y., Ounis, A., Hanocq, J.F., Moya, I., 2010. A field platform for continuous measurement of canopy fluorescence. IEEE Trans. Geosci. Remote Sens. 48, 3358–3368.

de Beurs, K.M., Henebry, G.M., 2005. Land surface phenology and temperature variation in the International Geosphere–Biosphere Program high-latitude transects. Glob. Chang. Biol. 11, 779–790.

De Jong, R., Verbesselt, J., Zeileis, A., Schaepman, M.E., 2013. Shifts in global vegetation activity trends. Remote Sens. 5, 1118–1133.

Delpierre, N., Dufrene, E., Soudani, K., Ulrich, E., Cecchini, S., Boe, J., et al., 2009. Modelling interannual and spatial variability of leaf senescence for three deciduous tree species in France. Agric. For. Meteorol. 149, 938–948.

Denning, A.S., Fung, I.Y., Randall, D., 1995. Latitudinal gradient of atmospheric CO_2 due to seasonal exchange with land biota. Nature 376, 240–243.

Fisher, J.B., Huntzinger, D.N., Schwalm, C.R., Sitch, S., 2014. Modeling the terrestrial biosphere. Annu. Rev. Environ. Resour. 39, 91–123.

Flexas, J., Escalona, J.M., Evain, S., Gulias, S.J., Moya, I., Osmond, C.B., et al., 2002. Steady-state chlorophyll fluorescence (Fs) measurements as a tool to follow variations of net CO_2 assimilation and stomatal conductance during water-stress in C3 plants. Physiol. Plant. 114 (2), 231–240.

Frankenberg, C., Fisher, J., Worden, J., Badgley, G., Saatchi, S., Lee, J.E., et al., 2011. New global observations of the terrestrial carbon cycle from GOSAT: Patterns of plant fluorescence with gross primary productivity. Geophys. Res. Lett. 38, L17706.

Frankenberg, C., O'dell, C., Berry, J., Guanter, L., Joiner, J., Kohler, P., Pollock, R., Taylor, T.E., 2014. Prospects for chlorophyll fluorescence remote sensing from the Orbiting Carbon Observatory-2. Remote Sens. Environ. 147, 1–12.

Fu, Y.H., Piao, S., Zhao, H., Jeong, S.J., Wang, X., Vitasse, Y., et al., 2014. Unexpected role of winter precipitation in determining heat requirement for spring vegetation green-up at northern middle and high latitudes. Glob. Change Biol. 20 (12), 3743–3755.

Fu, Y.H., Zhao, H., Piao, S., Peaucelle, M., Peng, S., Zhou, G., et al., 2015. Declining global warming effects on the phenology of spring leaf unfolding. Nature 526, 104–107.

Gonsamo, A., Chen, J.M., Price, D.T., Kurz, W.A., Wu, C., 2012. Land surface phenology from optical satellite measurement and CO_2 eddy covariance technique. J. Geophys. Res. 117, G03032. http://dx.doi.org/10.1029/2012JG002070.

Graven, H.D., Keeling, R.F., Piper, S.C., Patra, P.K., Stephens, B.B., Wofsy, S.C., et al., 2013. Enhanced seasonal exchange of CO_2 by Northern Ecosystems since 1960. Science 341, 1085–1089.

Guanter, L., Zhang, Y., Yung, M., Joiner, J., Voigt, M., Berry, J.A., et al., 2014. Global and time-resolved monitoring of crop photosynthesis with chlorophyll fluorescence. Proc. Natl. Acad. Sci. http://dx.doi.org/10.1073/pnas.1320008111.

Harris, I., Jones, P.D., Osborn, T.J., Lister, D.H., 2013. Updated high-resolution grids of monthly climatic observations - the CRU TS3.10 dataset. Int. J. Climatol. 34, 623–642.

Heffernan, J.B., Soranno, P.A., Angiletta, M.J., Buckley, L.B., Gruner, D.S., Keitt, T.H., et al., 2014. Macrosystem ecology: understanding ecological patterns and processes at continental scales. Front. Ecol. Environ. 12, 5–14.

Ho, C.H., Lee, E.J., Lee, I., Jeong, S.J., 2006. Earlier spring in Seoul, Korea. Int. J. Climatol. 26, 2117–2127.

Huete, A., Didan, K., Miura, T., Rodriguez, E.P., Gao, X., Ferreira, L.G., 2002. Overview of the radiometric and biophysical performance of the MODIS vegetation indices. Remote Sens. Environ. 83, 195–213.

Jeong, S.J., Medvigy, D., 2014. Macroscale prediction of autumn leaf coloration throughout the continental United States. Glob. Ecol. Biogeogr. 23, 1245–1254.

Jeong, S.-J., Ho, C.-H., Gim, H.-J., Brown, M.E., 2011. Phenology shifts at start vs. end of growing season in temperate vegetation over the Northern Hemisphere for the period 1982–2008. Glob. Chang. Biol. 17, 2385–2399.

Jeong, S.-J., Ho, C.-H., Choi, S.-D., Kim, J., Lee, E.-J., Gim, H.-J., 2013. Satellite data-based phenological evaluation of the nationwide reforestation of South Korea. PLoS One 8, e58900.

Joiner, J., Yoshida, Y., Vasilkov, A.P., Yoshida, Y., Corp, L.A., Middleton, E.M., 2011. First observations of global and seasonal terrestrial chlorophyll fluorescence from space. Biogeosciences 8 (3):637–651. http://dx.doi.org/10.5194/bg-8-637-2011.

Joiner, J., Guanter, L., Lindstrot, R., Voigt, M., Vasilkov, A.P., Middleton, E.M., Huemmrich, K.F., Yoshida, Y., Frankenberg, C., 2013. Global monitoring of terrestrial chlorophyll fluorescence from moderate spectral resolution near-infrared satellite measurements: methodology, simulations, and application to GOME-2. Atmos. Meas. Tech. 6:2803–2823. http://dx.doi.org/10.5194/amt-6-2803-2013.

Joiner, J., Yoshida, Y., Vasilkov, A.P., Schaefer, K., Jung, M., Guanter, L., et al., 2014. The seasonal cycle of satellite chlorophyll observations and its relationship to vegetation phenology and ecosystem-atmosphere carbon exchange. Remote Sens. Environ. 152, 375–391.

Jung, M., Reichstein, M., Margolis, H.A., Cescatti, A., Richardson, A.D., Arain, M.A., et al., 2011. Global patterns of land-atmosphere fluxes of carbon dioxide, latent heat, and sensible heat derived from eddy covariance, satellite, and meteorological observations. J. Geophys. Res. 116:G00J07. http://dx.doi.org/10.1029/2010JG001566.

Keeling, C.D., Chin, J.F.S., Whorf, T.P., 1996. Increased activity of vegetation inferred from atmospheric CO_2 measurements. Nature 382, 146–149.

Keenan, T.F., Gray, J., Friedl, M.A., Toomey, M., Bohrer, G., Hollinger, D.Y., et al., 2014. Net carbon uptake has increased through warming-induced changes in temperate forest phenology. Nat. Clim. Chang. 4, 598–604.

Kikuzawa, K., 2003. Phenological and morphological adaptations to the light environment in two woody and two herbaceous plant species. Funct. Ecol. 17, 29–38.

Krause, G.H., Weis, E., 1991. Chlorophyll fluorescence and photosynthesis: the basics. Annu. Rev. Plant Physiol. Plant Mol. Biol. 42, 313–349.

Lee, D.W., O'Keefe, J., Holbrook, N.M., et al., 2003. Pigment dynamics and autumn leaf senescence in a New England deciduous forest, eastern USA. Ecol. Res. 18, 677–694.

Lee, J.E., Frankenberg, C., van der Tol, C., Berry, J.A., Guanter, L., Boyce, C.K., et al., 2013. Forest productivity and water stress in Amazonia: observations from GOSAT chlorophyll fluorescence. Proc. R. Soc. B Biol. Sci.:280. http://dx.doi.org/10.1098/rspb.2013.0171.

Medvigy, D., Jeong, S.J., Clark, K.L., Skowronski, N.S., Schafer, K.V.R., 2013. Effects of seasonal variation of photosynthetic capacity on the carbon fluxes of a temperate deciduous forest. J. Geophys. Res. Biogeosci. 118, 1703–1714.

Melaas, E.K., Friedl, M.A., Zhu, Z., 2013. Detecting interannual variation in deciduous broadleaf forest phenology using Landsat TM/ETM+ data. Remote Sens. Environ. 132, 176–185.

Menzel, A., Sparks, T., Estrella, N., Roy, D., 2006. Altered geographic and temporal variability in phenology in response to climate change. Glob. Ecol. Biogeogr. 15, 498–504.

Meroni, M., Rossini, M., Guanter, L., Alonso, L., Rascher, U., Colombo, R., et al., 2009. Remote sensing of solar-induced chlorophyll fluorescence: review of methods and applications. Remote Sens. Environ. 113, 2037–2051.

Morin, X., Lechowicz, M.J., Augspurger, C., O'Keefe, J., Viner, D., Chuine, I., 2009. Leaf phenology in 22 North American tree species during the 21st century. Glob. Chang. Biol. 15, 961–975.

Myneni, R.B., Keeling, C., Tucker, C., Asrar, G., Nemani, R., 1997. Increased plant growth in the northern high latitudes from 1981 to 1991. Nature 386, 698–702.

Niu, S., Luo, Y., Fei, S., Montagnani, L., Bohrer, G., Janssens, I.A., et al., 2013. Seasonal hysteresis of net ecosystem exchange in response to temperature change: patterns and causes. Glob. Chang. Biol. 17, 3102–3114.

Park, H., Jeong, S.J., Ho, C.H., Kim, J., Brown, M.E., Schaepman, M.E., 2015. Nonlinear response of vegetation green-up to local temperature variations in temperate and boreal forests in the Northern Hemisphere. Remote Sens. Environ. 65, 100–108.

Piao, S., Mohammat, A., Fang, J., Cai, Q., Feng, J., 2006. NDVI-based increase in growth of temperate grasslands and its responses to climate changes in China. Glob. Environ. Chang. 16, 340–348.

Piao, S., Friedlingstein, P., Ciais, P., Viovy, N., Demarty, J., 2007. Growing season extension and its impact on terrestrial carbon cycle in the Northern Hemisphere over the past 2 decades. Glob. Biogeochem. Cycles 21, GB3018.

Piao, S., Tan, J., Chen, A., Fu, Y.H., Ciais, P., Liu, Q., et al., 2015. Leaf onset in the northern hemisphere triggered by daytime temperature. Nat. Commun. 6.

Pinzon, J.E., Tucker, C.J., 2014. A non-stationary 1981–2012 AVHRR NDVI3g time series. Remote Sens. 6, 6929–6960.

Richardson, A.D., Anderson, R.S., Arain, M.A., Barr, A.G., Bohrer, G., Chen, G., 2012. Terrestrial biosphere models need better representation of vegetation phenology: results from the North American Carbon Program site synthesis. Glob. Chang. Biol. 18, 566–584.

Richardson, A.D., Keenan, T.F., Migliavacca, M., Ryu, Y., Sonnentag, O., Toomey, M., 2013. Climate change, phenology, and phenological control of vegetation feedbacks to the climate system. Agric. For. Meteorol. 169, 156–173.

Running, S.W., Nemani, R.R., Heinsch, F.A., Zhao, M., Reeves, M., Hashimoto, H., 2004. A continuous satellite-derived measure of global terrestrial primary production. Bioscience 54, 547–560.

Schaefer, K., Schwalm, C.R., Williams, C., Arain, M.A., Barr, A., Chen, J.M., et al., 2012. A model-data comparison of gross primary productivity: results from the North American Carbon Program site synthesis. J. Geophys. Res. 117, G03010. http://dx.doi.org/10.1029/2012JG001960.

Schimel, D.S., Pavlick, R., Fisher, J.B., Asner, G.P., Saatchi, S., Townsend, P., et al., 2015. Observing terrestrial ecosystems and the carbon cycle from space. Glob. Chang. Biol. 21, 1762–1776.

Schwalm, C.R., Williams, C.A., Schaefer, K., Anderson, R., Arain, M.A., Baker, I., et al., 2010. A model-data intercomparison of CO_2 exchange across North America: results from the North American Carbon Program site synthesis. J. Geophys. Res. 115:G00H05. http://dx.doi.org/10.1029/2009JG001229.

Schwartz, M.D., Ahas, R., Aasa, A., 2006. Onset of spring starting earlier across the northern hemisphere. Glob. Chang. Biol. 12, 343–351.

Shen, M., Piao, S., Cong, N., Zhang, G., Jassens, I.A., 2015. Precipitation impacts on vegetation spring phenology on the Tibetan Plateau. Glob. Change Biol. 21 (10), 3647–3656.

Suni, T., Berninger, F., Markkanen, T., Keronen, P., Rannik, U., Vesala, T., 2003. Interannual variability and timing of growing season CO_2 exchange in a boreal forest. J. Geophys. Res. 108 (D9):4265. http://dx.doi.org/10.1029/2002JD002381.

Tucker, C.J., I.Y., Keeling, C.D., Gammon, R.H., 1986. Relationship between atmospheric CO_2 variations and a satellite-derived vegetation index. Nature 319, 195–199.

Van der Tol, C., Verhoef, W., Rosema, A., 2009. A model for chlorophyll fluorescence and photosynthesis at leaf scale. Agric. For. Meteorol. 149 (1), 96–105.

White, M.A., de Beurs, M.A., Didan, K., Inouye, D.W., Richardson, A.D., Jensen, O.P., et al., 2009. Intercomparison and interpretation of spring phenology in North America estimated from remote sensing for 1982 to 2006. Glob. Chang. Biol. 15, 2335–2359.

Wolkovich, E.M., Cook, B., Allen, J., Crimmins, T., Betancourt, J., Travers, S., et al., 2012. Warming experiments underpredict plant phenological responses to climate change. Nature 485, 494–497.

Xu, L., Myneni, R.B., Chapin III, F.S., Callaghan, T.V., Pinzon, J.E., Tucker, C.J., et al., 2013. Temperature and vegetation seasonality diminishment over northern lands. Nat. Clim. Chang. 3, 581–586.

Yang, X., Tang, J., Mustard, J.F., Lee, J.-E., Rossini, M., Joiner, J., et al., 2015. Solar-induced chlorophyll fluorescence that correlates with canopy photosynthesis on diurnal and seasonal scales in a temperate deciduous forest. Geophys. Res. Lett. 42, 2977–2987.

Yongshuo, H.F., Piao, S., Zhao, H., Jeong, S.-J., Wang, X., Vitasse, Y., Ciais, P., Janssens, I.A., 2014. Unexpected role of winter precipitation in determining heat requirement for spring vegetation green-up at northern middle and high latitudes. Glob. Chang. Biol. 20, 3743–3755.

Zarco-Tejada, P.J., Morales, A., Testi, L., Villalobos, F.J., 2013. Spatio-temporal patterns of chlorophyll fluorescence and physiological and structural indices acquired from hyperspectral imagery as compared with carbon fluxes. Remote Sens. Environ. 133, 102–115.

Zhang, Y., Guanter, L., Berry, J.A., Joiner, J., van der Tol, C., Huete, A., et al., 2014. Estimation of vegetation photosynthetic capacity from space-based measurements of chlorophyll fluorescence for terrestrial biosphere models. Glob. Chang. Biol. 20, 3727–3742.

Zhu, Z., Bi, J., Pan, Y., Ganguly, S., Anav, A., Xu, L., et al., 2013. Global data sets of vegetation leaf area index (LAI)3g and fraction of photosynthetically active radiation (FPAR)3g derived from global inventory modeling and mapping studies (GIMMS) normalized difference vegetation index (NDVI3g) for the period 1981 to 2011. Remote Sens. 5, 927–948.